J Sol-Gel Sci Technol (2016) 77:430–436
DOI 10.1007/s10971-015-3871-5

CrossMark

ORIGINAL PAPER

Thickness-dependent phase evolution and dielectric property of $Hf_{0.5}Zr_{0.5}O_2$ thin films prepared with aqueous precursor

Yong Yan[1] · Dayu Zhou[1,2] · Chunxia Guo[1] · Jin Xu[3] · Xirui Yang[1] · Hailong Liang[1] · Fangyang Zhou[1] · Shichao Chu[1] · Xiaoying Liu[1]

Received: 12 August 2015 / Accepted: 16 September 2015 / Published online: 1 October 2015
© Springer Science+Business Media New York 2015

Abstract $Hf_{0.5}Zr_{0.5}O_2$ thin films were prepared on silicon substrates by sol–gel method. The crystallization temperature, thickness, density, surface morphology, crystalline structure, and chemical bonding features of the films were investigated using TGA, DSC, XRR, AFM, GIXRD, and XPS techniques. The results showed that the crystallization temperature was 496 °C, the film surfaces were smooth and flat, and no pores and micro-cracks were discernable. The density increased significantly from 5.1 to 8.0 g/cm^3 after annealing at 700 °C. The crystalline structure depends strongly on the film thickness. The tetragonal phase could be stabilized in $Hf_{0.5}Zr_{0.5}O_2$ films thinner than 12.9 nm. An increase in the thickness led to a gradual appearance of the monoclinic phase, which ultimately became the dominant phase for films thicker than 46.1 nm. The results could be explained by the surface energy effect. Measured at 1 MV/cm, the leakage current density was about 3.5×10^{-6} A/cm^2, further indicating high quality of the thin films derived from aqueous solution precursor.

Graphical Abstract

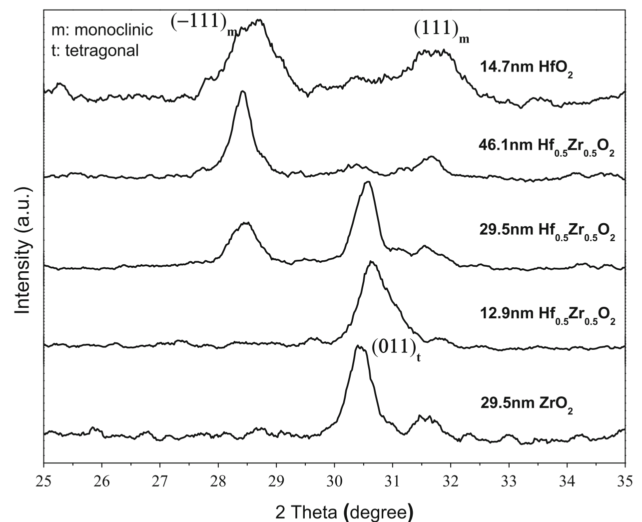

Keywords $Hf_{0.5}Zr_{0.5}O_2$ thin films · Aqueous precursor · Phase transition · Thickness dependence · Dielectric property

✉ Dayu Zhou
zhoudayu@dlut.edu.cn

1 Key Laboratory of Materials Modification by Laser, Ion, and Electron Beams (Ministry of Education), Dalian University of Technology, Dalian 116024, China

2 State Key Laboratory of Electronic Thin Films and Integrated Devices, University of Electronic Science and Technology of China, Chengdu 610054, China

3 Department of Electronic Engineering, Dalian Neusoft University of Information, Dalian 116023, China

1 Introduction

The transition metal oxides HfO_2- and ZrO_2-based high-permittivity (high-k) dielectric materials have been intensively studied and practically implemented in microelectronics [1, 2]. Pure HfO_2 transforms from monoclinic into tetragonal and cubic structures as temperature increases at ambient pressure. The application of HfO_2 with monoclinic phase has been limited since its dielectric constant is significantly lower than those of the cubic or tetragonal

phases. Therefore, making the high-permittivity phase to be stable at room temperature would be highly desirable. Efforts have been made to improve the properties of HfO_2 by adding different elements such as N, Si, Al, and La [3–6]. Addition of these elements helps to increase the crystallization temperature of HfO_2 and stability of the tetragonal or cubic phases, but sacrifices the k value due to the low permittivity of the dopants. ZrO_2 and HfO_2 have very similar crystal chemistry, and they are completely miscible. It has been shown that adding ZrO_2 into HfO_2 could stabilize the atomic layer deposition (ALD) process at high temperatures without lowering the dielectric constant, which was attributed to an increase in the tetragonal phase fraction in the crystalline films [7].

Pure and doped HfO_2 thin films can be prepared by various advanced vapor methods: atomic layer deposition [8, 9], chemical vapor deposition [10–12], and physical vapor deposition [13, 14]. In contrast to these techniques requiring sophisticated vacuum system, deposition of thin films by sol–gel method can enable the ease of composition control, high purity, large area coverage, as well as low cost. These advantages are especially preferred in fundamental study of material properties. Recently, Jiang et al. [15] reported a unique solution approach to depositing high-quality pure HfO_2 thin films using inorganic aqueous precursors. In comparison with conventional sol–gel routes using organic precursors [16–18], the coating can simply be operated in atmosphere condition, and especially, the very small size of sol particles (no larger than 2 nm) allow controllable growth of ultra-thin nano-films. In this paper, we extended this approach to preparing pure ZrO_2 and $Hf_{0.5}Zr_{0.5}O_2$ thin films, and the thickness-dependent phase evolution and dielectric properties have been investigated in detail.

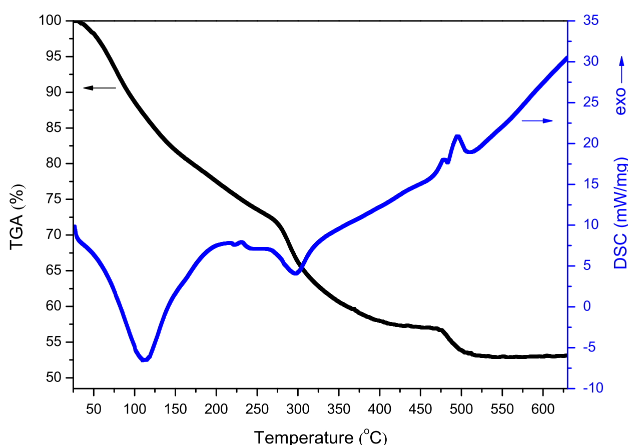

Fig. 1 TGA/DSC scans of $Hf_{0.5}Zr_{0.5}O_2$ precursor

2 Experimental

2.1 Precursor and film preparation

$HfOCl_2 \cdot 8H_2O$ (0.0048 mol) and $ZrOCl_2 \cdot 8H_2O$ (0.0048 mol) were dissolved in H_2O (40 mL) to ensure the Hf^{4+}:Zr^{4+} molar ratio of 1:1, followed by the addition of ammonia (0.0268 mol) to precipitate. The precipitate acquired was centrifuged and then washed with deionized water to remove Cl^- and ammonia. Finally, H_2O_2 (0.2 mol) and HNO_3 (0.0112 mol) were added into the precipitate and stirred to obtain a clear precursor solution. $Hf_{0.5}Zr_{0.5}O_2$ films were prepared by spin-coating the solution on 2 × 2 cm^2 p-type (100) silicon substrates with a low resistivity of 10^{-2}–10^{-3} Ω cm. All substrates received a modified RCA cleaning process with the native oxide layer being removed as the last step using diluted HF solution. After drying, the substrate surface was treated in air plasma for 10 min to make the contact angle of the solution of about 3° [19]. The solution was spin-coated at 3000 rpm for 30 s, followed by an immediate hot-plate polymerization at 150 °C for 30 s. Before the next coating, a 3-min air plasma treatment was carried out to improve the wettability of the film surface. This procedure was repeated until the desired thickness was obtained. Crystallization of the films was performed by 30-s rapid thermal annealing at 700 °C in a N_2 atmosphere.

2.2 Structural and chemical characterization

Thermogravimetric analysis (TGA) and differential scanning calorimetry (DSC) of the precursor were performed separately using Mettler-Toledo TGA/SDTA851e and Mettler-Toledo DSC822e in the temperature range of 25–630 °C under flowing argon. The heating rate was set as 10 K/min.

The surface morphology of the thin films was characterized by tapping mode atomic force microscopy (AFM, Bruker Innova) in area of 3 × 3 μm^2.

Grazing incidence X-ray diffraction (GIXRD) and X-ray reflectivity (XRR) data of $Hf_{0.5}Zr_{0.5}O_2$ thin films were measured on Bruker D8 Discover diffractometer with Cu K-alpha radiation (40 kV, 40 mA). For GIXRD, the incident beam was conditioned by using a 0.2-mm divergence slit. The exit beam was conditioned with a Soller slit. The incident angle was set to 0.5°. For XRR, the incident beam was conditioned by using a 0.2-mm divergence slit and the exit beam was conditioned with a 0.1-mm detector slit, respectively. The data were collected from 0.2° to 5° (2θ), with a step size of 0.002° and 0.5 s/step. Simulations and

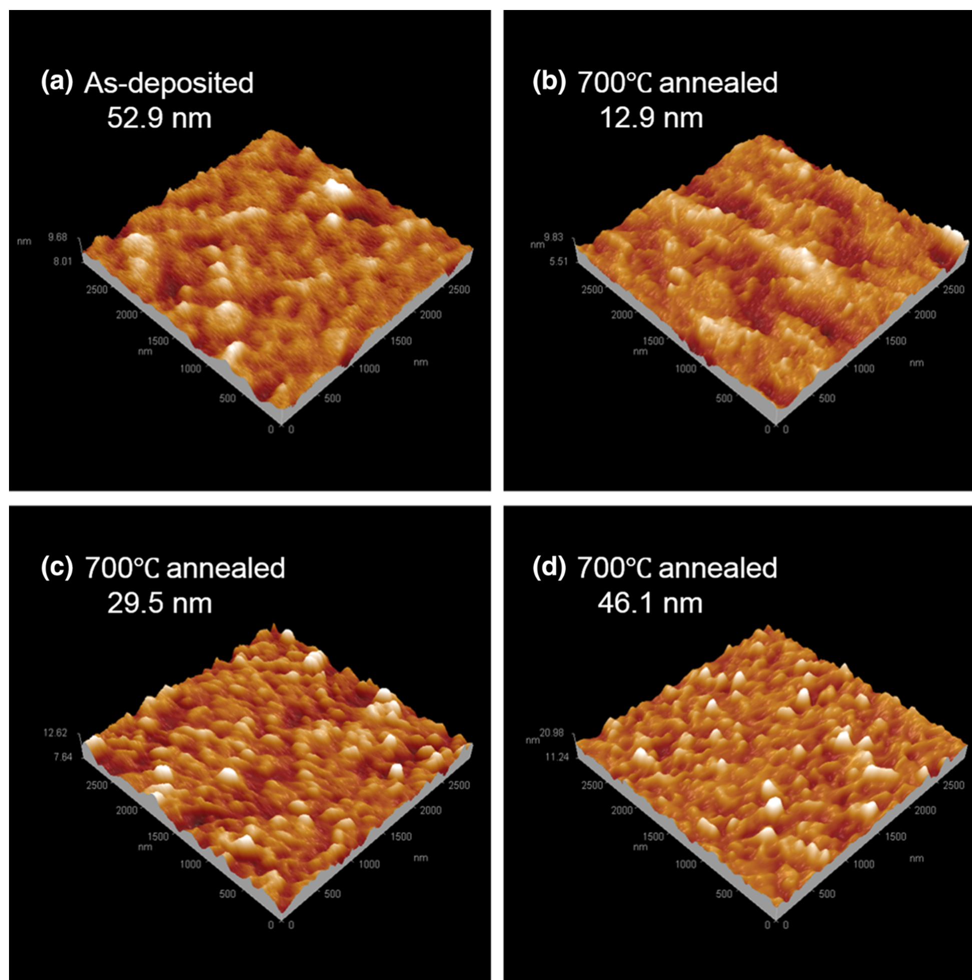

Fig. 2 AFM images for as-deposited (**a**) and 700 °C annealed (**b–d**) $Hf_{0.5}Zr_{0.5}O_2$ thin films illustrating the surface morphology affected by the annealing process and film thickness

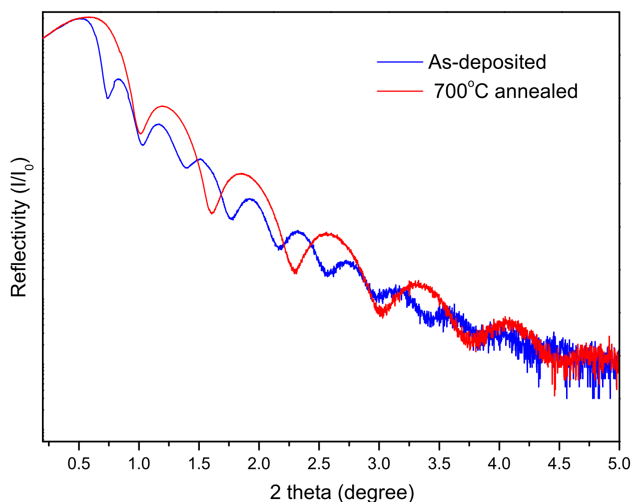

Fig. 3 XRR patterns for $Hf_{0.5}Zr_{0.5}O_2$ films with one coating cycle on Si (100) substrates before and after annealing at 700 °C

fitting of the XRR spectra were conducted by using DIFFRAC^{plus} LEPTOS analytical software to reveal the thickness, surface roughness, and density of the films.

Table 1 Model-fitting results for thickness, density, and roughness of $Hf_{0.5}Zr_{0.5}O_2$ films before and after annealing at 700 °C

Anneal (°C)	Thickness (nm)	Density (g/cm^3)	Roughness (nm)
Without	21.4	5.1	0.34
700	12.2	8.0	0.52

X-ray photoelectron spectroscopy (XPS) measurements were carried out using Thermo ESCALAB 250 X-ray photoelectron spectroscopy with an Al Ka X-ray source to probe the atomic ratio of hafnium and zirconium as well as the bonding features. XPS PEAKs 4.1 software was used to decompose and fit spectrum peaks.

For electrical characterization, TiN dots (100 μm radius) were deposited onto the crystallized films by DC reactive magnetron sputtering. The thickness of the TiN electrode was ~100 nm, and the resistivity was measured as about 75 μΩ cm. The polarization–electric field (P–E) and leakage current density–electric field (J–E) measurements were performed using the Multiferroic 100 V Test System (Radiant Technologies, USA) at room temperature. The TiN

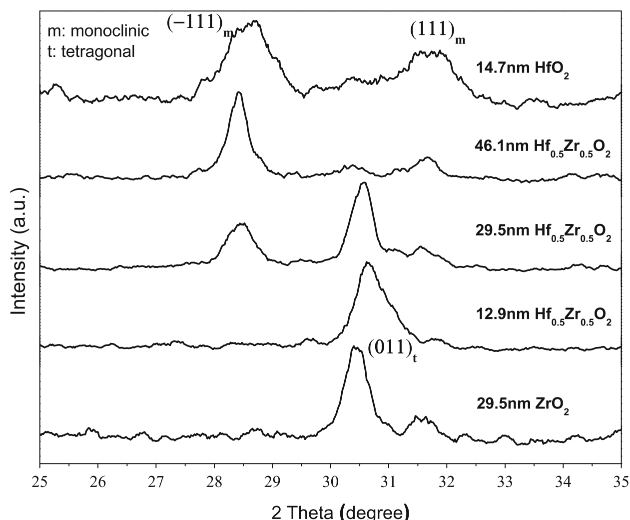

Fig. 4 GIXRD patterns of 700 °C annealed HfO_2, ZrO_2, and $Hf_{0.5}Zr_{0.5}O_2$ films with various thicknesses

dots were electrically stressed in measurements, and the low-resistivity Si substrate was grounded.

3 Results and discussion

3.1 TGA and DSC measurements

TGA and DSC data were recorded to gain insights into the decomposition chemistry of the $Hf_{0.5}Zr_{0.5}O_2$ precursor. To improve the resolution of the analysis, the precursor solution was preheated at 80 °C to volatilize most of the water. As seen from Fig. 1, several endotherm and exotherm peaks can be observed in the DSC curve, and each corresponds to a rapidest weight loss rate recorded by TGA. Referring to the decomposition chemistry analysis for pure HfO_2 aqueous precursor prepared using the same method [15], we attribute the first endotherm peak at 110 °C to a combined loss of the water and decomposition of the peroxo-groups from the solution. The second endotherm peak at 297 °C connects with nitrate decomposition. The exotherm peak at 496 °C should be attributed to the decomposition of tightly bounded hydroxyl species accompanied by crystallization.

3.2 AFM characterization

Figure 2 displays the AFM images for as-deposited and 700 °C annealed $Hf_{0.5}Zr_{0.5}O_2$ thin films grown on Si substrate. In general, the film surfaces are smooth and flat, and no pores and micro-cracks are discernable. The root-mean-square (RMS) surface roughness is only about 0.13 nm for as-deposited film. Annealing process leads to an increase in surface roughness, which are 0.40, 0.48, and 0.70 nm for films with thickness of 12.9, 29.5, and 46.1 nm. Additionally very smooth surface morphologies of all samples were also confirmed by scanning electron microscopy (data not shown here), and no noticeable grain and defects have been observed in SEM images of different magnification.

3.3 XRR studies

Figure 3 shows the XRR patterns for $Hf_{0.5}Zr_{0.5}O_2$ films with one coating cycle before and after annealing at 700 °C. By fitting the measured curves, their thickness, density, and surface roughness data were obtained and compared in Table 1. Annealing causes shrinkage and densification of the as-deposited thin films, resulting in a reduction in the thickness from 21.4 to 12.2 nm and an increase in the density from 5.1 to 8.0 g/cm^3. In addition, the observation of increasing surface roughness after annealing is consistent with the results from AFM measurement.

3.4 GIXRD determinations

GIXRD patterns of 700 °C annealed HfO_2, ZrO_2, and $Hf_{0.5}Zr_{0.5}O_2$ thin films with various thicknesses are shown in Fig. 4. The 29.5-nm-thick ZrO_2 and 14.7-nm-thick HfO_2 films were crystallized into pure tetragonal (t-) and pure monoclinic (m-) phases, respectively. An addition of ZrO_2 into HfO_2 helps to stabilize the t-phase; however, the t-phase stability at room temperature depends strongly on the film thickness. The 46.1-nm-thick $Hf_{0.5}Zr_{0.5}O_2$ film was crystallized mainly into m-phase, indicated by the m-(−111) and weak m-(111) peaks. When the thickness is reduced to 29.5 nm, the appearance of the t-(011) peak and weakening of the m-(−111) peak imply the film is composed by a mixture of the tetragonal and monoclinic phases. For the 12.9-nm-thick $Hf_{0.5}Zr_{0.5}O_2$ film, only the t-(011) peak at 30.5° exists, indicating that the film is crystallized mainly into t-phase. In $Hf_{0.5}Zr_{0.5}O_2$ films prepared by ALD, the monoclinic phase fraction was determined to be about 10 % [19].

Our result of film thickness-dependent monoclinic to tetragonal phase transition is in accordance with previous studies for HfO_2, ZrO_2, and HfO_2–ZrO_2 solid solution nano-films [7, 20–23], and the underlying mechanism should be attributed to the surface energy effect suggested firstly by Garvie [24]. For thin films with a large value of the molar surface, the thickness-dependent monoclinic to tetragonal phase transition temperature $\Delta T_{m\to t}(t)$ can be derived as:

$$\Delta T_{m\to t}(t) = T_{\text{bulk},m\to t} + \frac{2\alpha \cdot \Delta\gamma_{m\to t}}{bt},$$

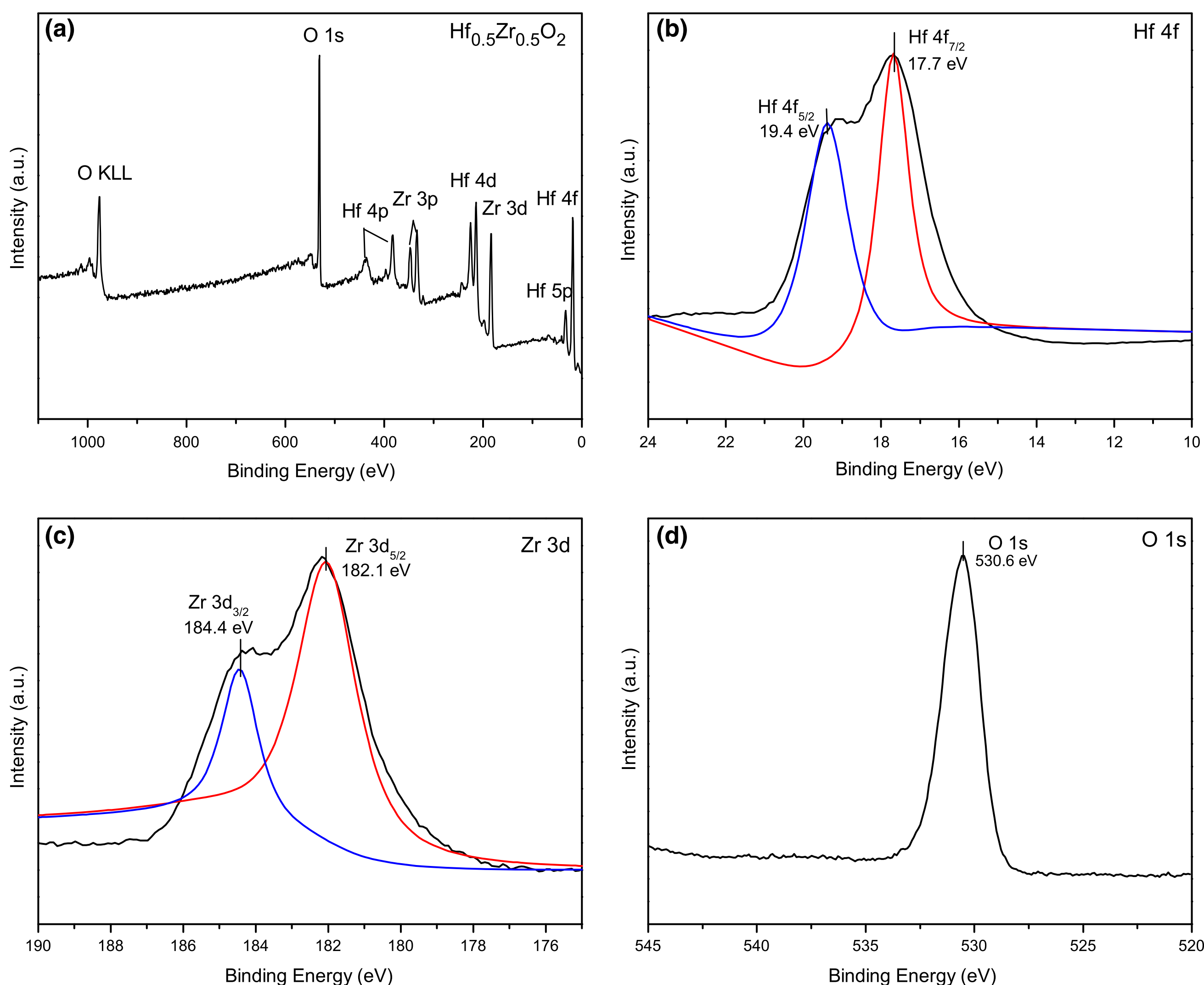

Fig. 5 **a** Low-resolution XPS spectrum of sol–gel-derived $Hf_{0.5}Zr_{0.5}O_2$ thin films annealed at 700 °C and **b–d** high-resolution XPS spectra of Hf 4*f*, Zr 3*d* and O 1*s* regions

where $T_{\text{bulk},\ m\rightarrow t}$ is monoclinic to tetragonal phase transition temperature of the bulk, α is a positive constant, t is the film thickness, $\Delta\gamma_{m\rightarrow t}$ is the change of surface energy, and b is the molar density. Parameters for ZrO_2: $T_{\text{bulk},\ m\rightarrow t} = 1430$ K; HfO_2: $T_{\text{bulk},\ m\rightarrow t} = 2066$ K [25].

Garvie [24] stated that the tetragonal ZrO_2 has a lower surface free energy than monoclinic ZrO_2, so $\Delta\gamma_{m\rightarrow t}$ is negative. b is positive. Thus, the monoclinic to tetragonal phase transition temperature $\Delta T_{m\rightarrow t}(t)$ decreases with a reduction in film thickness t. At a critical thickness, the tetragonal phase can be stabilized even at room temperature. Theoretical calculations give the critical thickness of approximate 15 nm for ZrO_2 and less than 2 nm for HfO_2 [26]. Note that ZrO_2 and HfO_2 have very similar crystal chemistry and are miscible completely. Therefore, the aforementioned surface energy effect discussion is also applicable for HfO_2–ZrO_2 solid solution thin films, and an intermediate critical thickness is expected. For our $Hf_{0.5}Zr_{0.5}O_2$ films, the critical thickness for t-phase stabilized at room temperature is around 12.9 nm, agreeing well with the expectation. It is worthy to mention that the crystal polymorph of the films is influenced strongly by many factors such as composition homogeneity, crystallization dynamics, defect type and density. They are acting either simultaneously or individually under different conditions. Thus, different film deposition methods and even the same preparation technique using different tools may cause inevitable variations in experimental critical thickness. For instance, the critical thickness of tetragonal $Hf_{0.5}Zr_{0.5}O_2$ films formed by ALD is less than 10 nm [7, 20, 21].

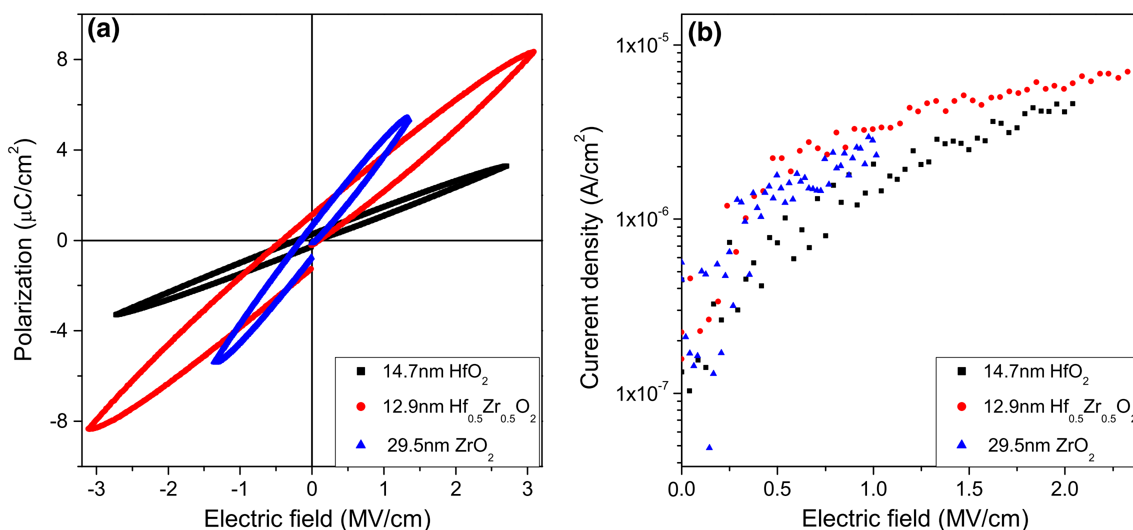

Fig. 6 Polarization–electric field curves measured at 4 V (**a**) and current density–electric field curves measured at 3 V (**b**) for HfO_2, $Hf_{0.5}Zr_{0.5}O_2$, and ZrO_2 films with various thicknesses

3.5 XPS analysis

Figure 5 shows low-resolution XPS spectrum of sol–gel-derived $Hf_{0.5}Zr_{0.5}O_2$ thin films annealed at 700 °C and high-resolution XPS spectra of Hf 4*f*, Zr 3*d*, and O 1*s* regions. For all the thin films analyzed, the binding energies were calibrated by setting carbon peak at 284.6 eV. In Fig. 5a, only peaks corresponding to Hf, Zr, and O elements are observed, but no other impurities (e.g., chloride ions) are involved. As shown in Fig. 5b, the Hf 4*f* spectrum consists of two components, i.e., the $4f_{7/2}$ part at 17.7 eV and the $4f_{5/2}$ part at 19.4 eV, which are in good agreement with the results of pure HfO_2 thin films derived also by sol–gel method [27]. Similarly, Fig. 5c shows that Zr 3*d* spectrum consists of two components, i.e., the $3d_{5/2}$ part at 182.1 eV and the $4f_{3/2}$ part at 184.4 eV, which agree well with those reported by Shimizu [28], whose films were derived by sol–gel as well. The O 1*s* spectrum is located at 530.6 eV (Fig. 5d). Accordingly, it can be concluded that the XPS analyses confirm the formation of Hf–O and Zr–O bonds in our films. In addition, the Hf and Zr contents were determined as 15.7 and 19.4 at.%, respectively, which is very close to the designed composition of $Hf_{0.5}Zr_{0.5}O_2$.

3.6 Electrical characterization

Figure 6 shows the electrical characterization results of HfO_2, ZrO_2, and $Hf_{0.5}Zr_{0.5}O_2$ thin films. Note that an application of the same 4 and 3 V potentials across the films with different thicknesses results in different electric fields. From the average gradient of polarization–electric field (*P–E*) curves in Fig. 6a, the relative dielectric permittivity (ε_r) can be calculated for three film samples, and the results are found to relate closely to their polymorphs. The monoclinic HfO_2 film has the lowest ε_r of 13.6, while the tetragonal ZrO_2 film has the highest ε_r of 42.1. For $Hf_{0.5}Zr_{0.5}O_2$, the ε_r is determined as 27.8, which is comparable to the same composition film prepared by ALD [7]. The intermediate permittivity of $Hf_{0.5}Zr_{0.5}O_2$ implies the existence of a small fraction of monoclinic phase in addition to the main tetragonal phase. Our experimental results agree well with theoretical prediction for HfO_2 that the dielectric constant increases with increasing crystal structure symmetry [29]. The reason of small hysteresis observed in *P–E* curves is still unclear, and perhaps there exist mobile ions and re-orientable vacancy defect dipoles in the film.

As shown in Fig. 6b, the leakage current densities of HfO_2, $Hf_{0.5}Zr_{0.5}O_2$, and ZrO_2 films are 2.4, 3.5, and 2.2×10^{-6} A/cm^2 measured at 1 MV/cm. The leakage current density is lower than HfO_2 thin films spin-coated using metal–organic reagent [30, 31], indicating high quality of our thin films derived from aqueous solution precursor.

4 Conclusions

In this work, stoichiometric $Hf_{0.5}Zr_{0.5}O_2$ thin films have been prepared on highly doped Si (100) substrates using inorganic aqueous precursor, followed by deposition of TiN electrode dots on top to measure the electrical properties. Rather smooth and dense $Hf_{0.5}Zr_{0.5}O_2$ thin films can be obtained after annealing at 700 °C. The XPS analyses confirm the formation of Hf–O and Zr–O bonds as well as atomic ratio of Hf and Zr approximating 1:1. The addition

of ZrO_2 helps to stabilize the tetragonal phase in HfO_2, and the stability depends strongly on film thickness. When the film thickness is below 12.9 nm, the $Hf_{0.5}Zr_{0.5}O_2$ films are crystallized mainly into tetragonal phase with a relative dielectric permittivity of 27.8 and leakage current density 3.5×10^{-6} A/cm^2 measured at 1 MV/cm.

Acknowledgments This work was supported by the National Natural Science Foundation of China (Grant No. NSFC 51272034) and the Open Research Fund of State Key Laboratory of Electronic Thin Films and Integrated Devices (UESTC) (No. KFJJ201101). The authors are responsible for the content of the paper.

References

1. Robertson J (2004) High dielectric constant oxides. Eur Phys J Appl Phys 28:265–291
2. Choi JH, Mao Y, Chang JP (2011) Development of hafnium based high-k materials—a review. Mater Sci Eng R 72:97–136
3. Akbar MS, Cho HJ, Choi R, Kang CS, Kang CY, Choi CH, Rhee SJ, Kim YH, Lee JC (2004) Optimized NH_3 annealing process for high-quality HfSiON gate oxide. IEEE Electron Device Lett 25:465–467
4. Tomida K, Kita K, Toriumi A (2006) Dielectric constant enhancement due to Si incorporation into HfO_2. Appl Phys Lett 89:2902
5. Park PK, Kang SW (2006) Enhancement of dielectric constant in HfO_2 thin films by the addition of Al_2O_3. Appl Phys Lett 89:2905
6. Mereu B, Dimoulas A, Vellianitis G, Apostolopoulos G, Scholz R, Alexe M (2005) Interface trap density in amorphous $La_2Hf_2O_7/SiO_2$ high-k gate stacks on Si. Appl Phys A 80:253–257
7. Müller J, Böscke TS, Schröder U, Reinicke M, Oberbeck L, Zhou D, Weinreich W, Kücher P, Lemberger M, Frey L (2009) Improved manufacturability of ZrO_2 MIM capacitors by process stabilizing HfO_2 addition. Microelectron Eng 86:1818–1821
8. Aarik J, Aidla A, Kiisler AA, Uustare T, Sammelselg V (1999) Influence of substrate temperature on atomic layer growth and properties of HfO_2 thin films. Thin Solid Films 340:110–116
9. Aarik J, Aidla A, Mandar H, Uustare T, Kukli K, Schuisky M (2001) Phase transformations in hafnium dioxide thin films grown by atomic layer deposition at high temperatures. Appl Surf Sci 173:15–21
10. Balog M, Schieber M, Patai S, Michman M (1972) Thin films of metal oxides on silicon by chemical vapor deposition with organometallic compounds. I. J Cryst Growth 17:298–301
11. Williams PA, Jones AC, Tobin NL, Chalker PR, Taylor S, Marshall PA, Critchlow GW (2003) Growth of hafnium dioxide thin films by liquid-injection MOCVD using alkylamide and hydroxylamide precursors. Chem Vap Depos 9:309–314
12. Jones AC, Chalker PR (2003) Some recent developments in the chemical vapour deposition of electroceramic oxides. J Phys D Appl Phys 36:R80
13. Pereira L, Barquinha P, Fortunato E, Martins R (2005) Influence of the oxygen/argon ratio on the properties of sputtered hafnium oxide. Mater Sci Eng B118:210–213
14. Hu H, Zhu C, Lu YF, Wu YH, Liew T, Li MF, Cho BJ, Choi WK, Yakovlev N (2003) Physical and electrical characterization of HfO_2 metal–insulator–metal capacitors for Si analog circuit applications. J Appl Phys 94:551–557
15. Jiang K, Anderson JT, Hoshino K, Li D, Wager JF, Keszler DA (2011) Low-energy path to dense HfO_2 thin films with aqueous precursor. Chem Mater 23:945–952
16. Zaharescu M, Teodorescu VS, Gartner M, Blanchin MG, Barau A, Anasescu M (2008) Correlation between the method of preparation and the properties of the sol–gel HfO_2 thin films. J Non-Cryst Solids 354:409–415
17. Wang KJ, Cheong KY (2008) Investigation of sol–gel derived HfO_2 on 4H-SiC. Appl Surf Sci 254:1981–1985
18. Shimizu H, Nemoto D, Ikeda M, Nishide T (2010) Characteristics of sol–gel-derived and crystallized HfO_2 thin films dependent on sol solution. Jpn J Appl Phys 49:121502
19. Müller J, Böscke TS, Schröder U, Mueller S, Bräuhaus D, Böttger U, Mikolajick T (2012) Ferroelectricity in simple binary ZrO_2 and HfO_2. Nano Lett 12:4318–4323
20. Park MH, Kim HJ, Kim YJ, Lee W, Moon T, Hwang CS (2013) Evolution of phases and ferroelectric properties of thin $Hf_{0.5}Zr_{0.5}O_2$ films according to the thickness and annealing temperature. Appl Phys Lett 102:242905
21. Triyoso DH, Hegde RI, Schaeffer JK, Roan D, Tobin PJ, Samavedam SB, White JBE (2006) Impact of Zr addition on properties of atomic layer deposited HfO_2. Appl Phys Lett 88:2901
22. Shandalov M, Mclntyre PC (2009) Size-dependent polymorphism in HfO_2 nanotubes and nanoscale thin films. J Appl Phys 106:084322
23. Böscke TS, Hung PY, Kirsch PD, Quevedo-Lopez MA, Ramírez-Bon R (2009) Increasing permittivity in HfZrO thin films by surface manipulation. Appl Phys Lett 95:052904
24. Garvie RC (1965) The occurence of metastable tetragonal zirconia as a crystalline size effect. J Phys Chem 69:1238–1243
25. Wang C, Zinkevich M, Aldinger F (2006) The zirconia–hafnia system: DTA measurements and thermodynamic. J Am Ceram Soc 89:3751–3758
26. Navrotsky A (2005) Thermochemical insights into refractory ceramic materials based on oxides with large tetravalent cations. J Mater Chem 15:1883–1890
27. Brezesinski T, Smarsly B, Iimura KI, Grosso D, Boissière C, Amenitsch H, Sanchez C (2005) Self-assembly and crystallization behavior of mesoporous, crystalline HfO_2 thin films: a model system for the generation of mesostructured Transition–Metal Oxides. Small 1:889–898
28. Shimizu H, Nishide T (2012) Characterization of sol–gel-derived and crystallized HfO_2, ZrO_2, ZrO_2–Y_2O_3 thin films on Si (001) wafers with high dielectric constant. In: Mastai Y (ed) Advances in crystallization processes, chap. 13. InTech, Rijeka
29. Zhao Xinyuan, Vanderbilt David (2002) First-principles study of structural, vibrational, and lattice dielectric properties of hafnium oxide. Phys Rev B 65:233106
30. Wang ZJ, Kumagai T, Kokawa H, Tsuaur J, Ichiki M, Maeda R (2005) Crystalline phases, microstructures and electrical properties of hafnium oxide films deposited by sol–gel method. J Cryst Growth 281:452–457
31. Yu JJ, Fang Q, Zhang JY, Wang ZM, Boyd IW (2003) Hafnium oxide layers derived by photo-assisted sol–gel processing. Appl Surf Sci 208:676–681